Revisiting the recollisional excitation-tunneling process in strong-field nonsequential double ionization of helium

Zhangjin Chen, Yali Wang, Toru Morishita, Xiaolei Hao, Jing Chen, Oleg Zatsarinny, and Klaus Bartschat

Revisiting the recollisional excitation-tunneling process in strong-field nonsequential double ionization of helium

Zhangjin Chen and Yali Wang

Department of Physics, College of Science, Shantou University,
Shantou, Guangdong 515063, People's Republic of China

Toru Morishita

Institute for Advanced Science, The University of Electro-Communications,
1-5-1 Chofu-ga-oka, Chofu-shi, Tokyo 182-8585, Japan

Xiaolei Hao

Institute of Theoretical Physics and Department of Physics,
Shanxi University, Taiyuan 030006, People's Republic of China

Jing Chen

Institute of Applied Physics and Computational Mathematics,
P. O. Box 8009, Beijing 100088, People's Republic of China and
Center for Advanced Material Diagnostic Technology, College of Engineering Physics,
Shenzhen Technology University, Shenzhen 518118, People's Republic of China

Oleg Zatsarinny and Klaus Bartschat

Department of Physics and Astronomy, Drake University, Des Moines, Iowa 50311, USA
(Dated: July 15, 2019)

We revisit the excitation-tunneling process in nonsequential double ionization (NSDI) of helium in an 800 nm laser field. The correlated two-electron momentum distributions are calculated by using the improved quantitative rescattering (QRS) model, in which the lowering of the threshold energy due to the presence of an electric field at the instant of recollision is taken into account. In the framework of the QRS model, the correlated two-electron momentum distributions for excitation-tunneling in NSDI can be factorized as a product of the returning-electron wave packet (RWP) and the field-free differential cross section (DCS) for electron impact excitation of the parent ion multiplied by the tunneling ionization rate of electrons in the excited states. The RWPs, which describe the momentum distribution of the returning electrons, are obtained within the strong-field approximation for high-order above-threshold ionization. The DCSs for electron impact excitation of He^+ are calculated using the state-of-the-art many-electron R-matrix theory, and the tunneling ionization rates for electrons in the excited states are evaluated by solving the time-dependent Schrödinger equation. The calculated correlated two-electron momentum distribution shows that the fourfold symmetry with regard to the parallel momentum components is broken. This is in contradiction to the prevalent view that the correlation pattern for excitation-tunneling in NSDI is symmetric with respect to the coordinate axes. By including the recollisional $(e, 2e)$ process, the predicted correlated two-electron momentum distributions are found to be in good qualitative agreement with experiment.

PACS numbers: 32.80.Fb, 32.80.Rm, 34.50.Rk, 34.80.Dp

I. INTRODUCTION

The controversial debate on the mechanisms responsible for nonsequential double ionization (NSDI) was already settled by the early measurements of the total yield of doubly charged ions as a function of the laser intensity [1] and the recoil-ion momentum distributions [2, 3]. Now it is widely accepted that NSDI is one of the laser-induced rescattering processes that support the classical recollision model [4]. However, since total ion yields or ion momentum distributions alone do not provide detailed information on the physics behind NSDI, coincidence measurements of correlated two-electron momentum distribution are very attractive. A kinematical analysis of the measured two-electron momentum distribution for NSDI of Ar within the classical "recollision model" revealed an $(e, 2e)$-like process and excitation with subsequent tunneling of the second electron as two different ionization mechanisms [5].

Since the pioneering measurements of the correlated two-electron momentum distributions (CMD) for NSDI of Ar, carried out at the turn of this century [6], a number of experiments on CMD have been performed [7–12]. Among those, the measurement with high resolution and good statistics on NSDI of helium in a strong laser pulse at 800 nm by Staudte *et al.* [7] is of special interest. The prominent fingerlike structure observed in the latter study has been investigated by various theoretical

models, including a semiclassical quasistatic model [13], a classical three-dimensional ensemble model [14], our own quantitative rescattering (QRS) model [15], as well as *ab initio* calculations by solving the time-dependent Schrödinger equation (TDSE) also reported in [7]. Although serious discrepancies exist between the calculated results and the experimental data, all these theoretical studies attributed the fingerlike structure to a laser-induced $(e, 2e)$ recollision process, in which the final-state electron-electron repulsion plays an important role. The above theoretical studies, indeed, focused on the electron impact ionization mechanism. Another physical mechanism, recollisional excitation with subsequent tunneling, has been studied much less. In the recollisional excitation-tunneling process, the returning electron does not provide the second electron with enough energy to be released into the continuum. Instead, the electron is excited to another bound state, from which it is subsequently ionized via tunneling.

The recollisional excitation-tunneling in NSDI of helium exposed to a strong laser pulse at 800 nm [7] was specifically studied in our previous work [19]. We employed the QRS model based on the factorization formula in Ref. [20]. The QRS model was originally proposed to describe the photoelectrons in high-order above-threshold ionization (HATI) attributed to laser-induced elastic scattering of the returning electron from the parent ion [16, 17]. It was later applied to other rescattering processes such as high-order harmonic generation [18] and NSDI [15, 19, 21] due to recombination and inelastic scattering of the returning electron with the parent ion, respectively. According to the QRS model, the CMD for recollisional excitation-tunneling in NSDI can be expressed as a product of the differential cross section (DCS) for electron-impact excitation and the ionization rate for tunneling ionization of the second electron from the excited state, multiplied by the returning electron wave packet to indicate the weight of the contribution at each incident energy. Within the QRS model, numerical simulations of the CMD for recollisional $(e, 2e)$ and excitation-tunneling are performed separately. Therefore, the simulated results for excitation-tunneling were compared directly with the corresponding portion of experimental data reported in [19], where the excitation-tunneling portion of the experimental data was extracted from the original measurements [7] based on the assumption that the CMD for excitation-tunneling is symmetric with respect to the coordinate axes [5].

In our previous work [19], the DCSs for electron impact excitation of He^+ was calculated using the distorted-wave Born approximation (DWBA), while the parallel momentum distribution for tunneling-ionization was evaluated using the modified ADK (Ammosov-Delone-Krainov) [22] model proposed by Tong and Lin [23]. Even though the angular distribution of the DCS from DWBA calculations is typically in fairly good agreement with experiment, it is well known that, at low energies, the total cross sections predicted by the DWBA often exceed the experimental values significantly. Consequently, the DCSs from DWBA-based models are also larger than the absolute experimental data [24]. On the other hand, when the modified ADK model is employed to simulate the parallel momentum distribution for tunneling-ionization, an accurate absolute ionization rate is highly desirable, since its value affects the shape of the parallel momentum distribution significantly.

Unfortunately, a damping factor was introduced empirically in the modified ADK model. Although the damping factor was estimated for ionization from the ground state of a few atoms and ions, by fitting ionization rates calculated accurately using the complex scaling method [25, 26], it is (to our knowledge) not available for ionization from excited states. As a matter of fact, our own tests revealed that the ionization rates for ionization from excited states of ions are very sensitive to the choice of the damping factor. This suggests that the ionization rate for tunneling-ionization cannot be evaluated unambiguously in NSDI, if the modified ADK model is employed. Even if accurate ionization rates can be obtained from the modified ADK model, the results do not provide the transition amplitude, which is required in the study of quantum interference effects in NSDI at low intensities [27–29].

In this paper, we revisit the recollisional excitation-tunneling process in helium using the improved QRS model [30, 31], in which the reduction of the kinetic energy required for the electrons to escape from the parent ion due to the presence of the electric field at the instant of recollision [32] has been taken into account. The DCSs for electron impact excitation of He^+ ion are calculated using the state-of-the-art many-electron R-matrix method to solve the resulting close-coupling equations, while the tunneling ionization rate of electrons in the excited states are evaluated by solving the TDSE within the single-active-electron approximation [33]. We expect our approach to result in one of the most accurate simulations of the CMD for the recollisional excitation-tunneling process. While this theoretical treatment also enables the QRS model to be used to investigate the quantum interference effect in NSDI, this aspect is irrelevant for the case considered here.

Unless indicated otherwise, atomic units (a.u.) are used throughout this manuscript.

II. NUMERICAL PROCEDURES

We consider excitation-tunneling of He in a linearly polarized laser pulse with its electric field along the z axis. At a single peak intensity (i.e., no focal-volume averaging, which we assume in this manuscript unless specified otherwise), the CMD can be expressed as a product of the parallel momentum distribution for the scattered electron after recollisional excitation and the parallel momentum distribution for tunneling-ionized electrons from the excited states.

For the laser-induced recollisional process of He$^+$ considered here, the two electrons involved in the process start in the singlet ground state of He, and their singlet coupling is preserved during the recollisional process since the absorption of photons does not affect the total spin [34]. Thus we only need to consider the singlet scattering cross sections. In the CMD for NSDI, the experimental data are measured only for the momentum components of the two electrons along the laser polarization axis. Thus, to compare with experiment, one needs to project the singlet DCS $d\sigma^s/d\Omega$ for electron impact excitation of He$^+$ onto the polarization direction. The parallel momentum distribution for the scattered electron after recollisional excitation is given by

$$Y_{E_i}^{\text{excit}}(k_1^{||}) = \frac{2\pi}{k_1} \frac{d\sigma^s}{d\Omega}. \tag{1}$$

In Eq. (1), E_i is the energy of the incident (returning) electron, k_1 is the momentum of the scattered electron, and $k_1^{||} = k_1 \cos\theta$, where θ is the scattering angle with respect to the direction of the returning electron. The DCSs are calculated with the nonperturbative close-coupling with pseudo-states method using the fully parallelized B-spline R-matrix code [35]. Note that the integration over the perpendicular components was performed in Eq. (1).

Suppose the laser-induced recollisional excitation process occurs at t_r when the vector potential $\boldsymbol{A}_r = \boldsymbol{A}(t_r)$. As a result of the projectile electron still being under the influence of the laser field after the collision, the electron will gain an additional momentum $-A_r$ in the direction of the laser polarization from t_r to the end of the laser pulse. Therefore, the corresponding parallel momentum distribution for the recollisional excitation process in a strong field at an intensity I can be obtained from Eq. (1) by shifting the momentum of the projectile electron by $-A_r$, i.e.,

$$D_{E_i,I}^{\text{excit}}(p_1^{||}) = Y_{E_i}^{\text{excit}}(k_1^{||} - A_r). \tag{2}$$

The vector potential A_r in Eq. (2) is related to the momentum k_r of the returning electron. The relation between k_r and A_r can be determined by solving the one-dimensional Newton equation for the motion of the tunneled electron in the electric field without taking into account the Coulomb potential. For a monochromatic laser field $\boldsymbol{F}(t) = \hat{z}F_0 \cos(\omega t)$, the calculation shows that the mean value of k_r/A_r is about 1.25 in the returning range of $240° < \omega t_r < 320°$, corresponding to tunneling ionization times resulting in $2° < \omega t_i < 22°$ [16]. Outside of that range, the electron yield is very small.

In the QRS model, we simply take

$$|A_r| = k_r/1.26. \tag{3}$$

The validity of Eq. (3) has been extensively verified in the description of laser-induced electron diffraction due to elastic scattering of the electron from the parent ion [16,

17, 36–39]. We note that the factorization formula near the outermost backward rescattering caustic was recently derived from adiabatic theory [40].

However, for laser-induced electron impact excitation of the parent ion in NSDI, Eq. (3) needs to be modified to account for the lowering of the threshold energy due to the presence of the electric field. In a free atom or ion, an incoming electron can promote the ground-state electron to an excited state and remain a continuum electron only when its kinetic energy is larger than the energy difference between the ground state and the excited state, since the total energy of a continuum electron must be positive. Nevertheless, in the presence of an electric field, the combined atomic and electric potentials form a barrier below zero, indicating that the projectile electron can escape from the atom or ion even with negative energy as long as its energy is higher than the potential barrier [32]. Therefore, in the laser-induced recollision process, electron impact excitation of the parent ion can still take place even when the returning electron has an energy less than the energy difference between the ground state and the excited state. This phenomenon is usually referred to as "lowering of threshold". This does not mean, however, that the energy level of an excited state is lowered. Since He$^+$ is a hydrogen-like ion with nuclear charge $Z=2$, the energy levels are $-Z^2/2n^2$, where n is the principal quantum number.

The maximum barrier height in the combined Coulomb and electric field potentials is given by [32]

$$V_b = -2\sqrt{Z_{\text{eff}}|F_r|}, \tag{4}$$

where Z_{eff} is the effective charge of the Coulomb potential seen by the projectile electron asymptotically, and F_r is the electric field at the instant of collision. For electron impact excitation of a singly-charged ion, $Z_{\text{eff}} = 1$. Therefore, the threshold is lowered by

$$\Delta E = 2\sqrt{|F_r|}. \tag{5}$$

However, since the barrier height of the combined atomic and electric field varies with the time the laser-induced electron returns to the origin, we choose an "average" returning time to make the calculations tractable. The method used to determine the average returning time was described in Ref. [41]. For example, in an 800 nm laser field at a peak intensity of 3.5×10^{14} W/cm^2, the threshold is lowered by $\Delta E = 10$ eV.

Unfortunately, it is still a formidable task to perform actual numerical calculations with the lowering of threshold included. Alternatively, van der Hart and Burnett [32] suggested that, to account for the lowering of threshold, one should adjust the collision energy so that the returning electron energy E_r ($= E_i$) corresponds to the incoming energy $E_r + \Delta E$ for electron impact excitation in the field-free case. Taking again the 800 nm laser field at a peak intensity of 3.5×10^{14} W/cm^2 as an example, the maximum energy of the laser-induced returning electron, determined by the classical rescattering model,

is $3.17U_p = 67$ eV (where U_p is the ponderomotive energy). This maximum recollision energy corresponds to the incident energy of 77 eV in the laser-free scattering process. Consequently, Eq. (3) should be rewritten as

$$|A_r| = \sqrt{2(E_i - \Delta E)}/1.26. \qquad (6)$$

With this improvement, the QRS model has been successfully applied to NSDI processes in calculations of the total yield of doubly-charged ions as a function of laser intensity [30, 31].

Next, we evaluate the parallel momentum distribution for tunneling ionization of electrons in the excited states. Due to the limitations of the modified ADK model [23] mentioned in the previous section, we solve the TDSE directly in the present work by using a second-order split-operator method (for details, see Refs. [33, 42]). First, we calculate the two-dimensional (2D) momentum distributions for single ionization of electrons from excited states with a specified magnetic quantum number. Then the parallel momentum distributions for the tunneling-ionized electrons are obtained by integrating the 2D momentum distributions over the momentum component perpendicular to the laser polarization.

With the parallel momentum distributions $D_{E_i,I}^{\text{excit}}(p_1^{||})$ calculated by using Eq. (2) for excitation and $D_I^{\text{tun}}(p_2^{||})$ by solving the TDSE for tunneling ionization, the CMDs for laser-induced electron impact excitation at incident energy E_i with subsequent tunneling ionization in the laser field at a peak intensity I are obtained as

$$D_{E_i,I}(p_1^{||}, p_2^{||}) = D_{E_i,I}^{\text{excit}}(p_1^{||}) \times D_I^{\text{tun}}(p_2^{||}). \qquad (7)$$

For a given intensity, in principle, excitation takes place as long as the kinetic energy of the returning electron is larger than the lowered threshold energy. Therefore, an integral over E_i should be performed to account for the contributions from collisions at all incident energies. This gives

$$D_I(p_1^{||}, p_2^{||}) = \int_{I_p - \Delta E}^{\infty} dE_i D_{E_i,I}(p_1^{||}, p_2^{||}) W_I(E_i), \qquad (8)$$

where I_p is the threshold energy for excitation, and $W_I(E_i)$ is the wave packet describing the energy (momentum) distributions of the returning (incoming) electron in the laser field at an intensity I [16], which indicates the weight of the contribution at incident energy E_i. The returning electron wave packet can be calculated by using the second-order strong-field approximation for HATI. For He, details of the calculations for the returning electron wave packet were presented in Ref. [30].

Nevertheless, the correlated two-electron momentum distributions generated using Eq. (8) may not be used to directly compare with the experimental measurements until the focal volume effect has been taken into account. This is due to the well-known fact that the intensity distribution of a focused laser beam is not uniform in space,
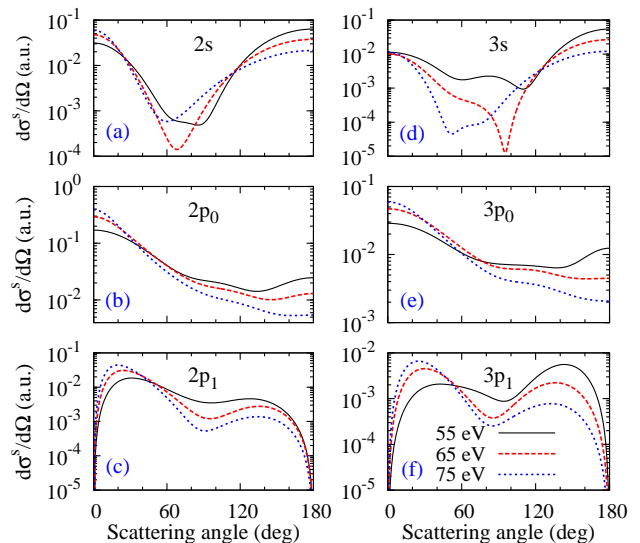

FIG. 1: Singlet differential cross sections for electron impact excitation of He$^+$ from the ground state to the excited states of (a) $2s$, (b) $2p_0$, (c) $2p_1$, (d) $3s$, (e) $3p_0$, and (f) $3p_1$, at incident energies of 55, 65, and 75 eV, respectively.

and the atoms located anywhere in the interaction volume experience different peak intensities. Therefore, to compare with experiment, an integration over the focus volume should be performed according to

$$D_{I_0}(p_1^{||}, p_2^{||}) = \int_0^{I_0} D_I(p_1^{||}, p_2^{||}) V(I) \, dI. \qquad (9)$$

Here I_0 is the peak intensity of the laser field, and $V(I)$ is the volume of an isointensity shell. For a laser beam with a Lorentzian distribution in the propagation direction and a Gaussian distribution in the transverse direction, the volume of an isointensity shell was given by Augst et al. [43].

III. RESULTS AND DISCUSSION

We aim to simulate the CMD for recollisional excitation-tunneling of He in 45 fs (FWHM of the intensity) linearly-polarized laser pulses at 800 nm [7]. For this purpose, we need to calculate the parallel momentum distributions for the projectile electron after laser-induced recollision and for the electron tunneling-ionized from excited states, as well as the wave packet for the laser-induced returning electron.

To obtain the parallel momentum distributions for the projectile electron after laser-induced recollision, we first calculate the singlet DCSs for electron impact excitation of He$^+$ from the ground state to the excited states of $n = 2$ and $n = 3$ for each angular momentum l with specific magnetic quantum number m, respectively. [We use the short-hand notation $2p_0 \equiv 2p\,(m = 0)$ and similarly for $2p_1$, $3p_0$, $3p_1$.] In Figure 1, we show the calculated
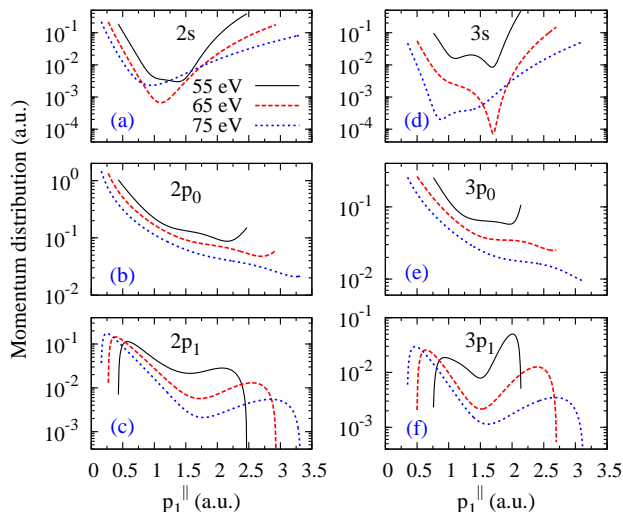
FIG. 2: Parallel momentum distributions for the active electron after recolliding with the He$^+$ ion and exciting the residual ground-state electron to the excited states of (a) $2s$, (b) $2p_0$, (c) $2p_1$, (d) $3s$, (e) $3p_0$, and (f) $3p_1$ at energies of 55, 65, and 75 eV in an 800 nm laser field at a peak intensity of 3×10^{14} W/cm^2. The recolliding electron returns along the $-\hat{z}$ direction.

FIG. 3: (a) Two-dimensional photoelectron momentum distributions (on a logarithmic scale) parallel ($p_{||}=p_z$) and perpendicular ($p_\perp=\sqrt{p_x^2 + p_y^2}$) to the laser polarization direction for single ionization of He$^+$ from the excited $2p_0$ state in an 800 nm laser field at the intensity of 2.5×10^{14} W/cm^2; (b) Same as (a) but for $3p_0$; (c) Electric field used in the TDSE calculations. The half circles in (a) and (b) indicate the photoelectron energy of $2U_p$.

DCSs using the R-matrix method for some selected excited states. As expected, excitation to $2p_0$ dominates. For the incident energies considered here, the DCSs for excitation to the $2s$ and $3s$ states exhibit strong backward scattering, which is comparable to or even higher than forward scattering, while those for $2p_0$ and $3p_0$ decrease rapidly as the scattering angle increases. Interestingly, the DCSs for excitation to $2p_1$ and $3p_1$ are very small near both the forward and backward directions for scattering angles smaller than 20° and larger than 160°, respectively.

The parallel momentum distributions for the projectile electron after laser-induced recollision are obtained by projecting the singlet DCSs for electron impact excitation of He$^+$ onto the polarization direction using Eq. (1) and shifting the parallel momentum by $-A_r$ according to Eq. (2). Figure 2 displays the parallel momentum distributions for the returning electron after the collision, corresponding to the singlet DSCs shown in Fig. 1, in the laser field at a peak intensity of 3×10^{14} W/cm^2. According to the classical rescattering model, the parallel momentum of the scattered electron after the laser-induced recollision is restricted by [5]

$$-\sqrt{2(E_i - I_p)} - A_r \leq p_1^{||} \leq \sqrt{2(E_i - I_p)} - A_r. \quad (10)$$

The above equation implies that the range of the momentum distribution shrinks as the excitation energy increases. Consequently, as seen in Fig. 2, the momentum distributions for $n = 3$ cover smaller ranges compared to those for $n = 2$. It should be noted that, in the im-
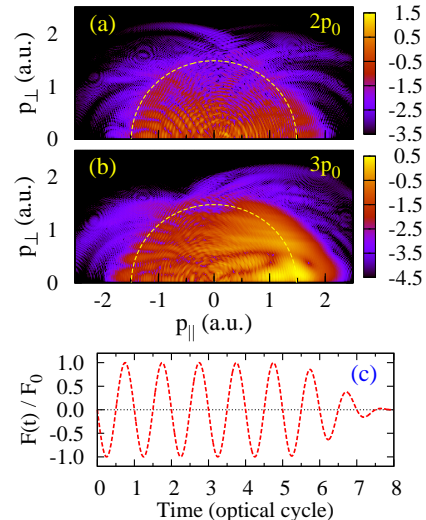
proved QRS model, the momentum shift $|A_r|$ depends on the laser intensity when the lowering of threshold energy is taken into account. Consequently, compared to the results obtained using the original QRS model [19], the parallel momentum distributions for the scattered electron shift to smaller momentum by

$$\Delta A_r = \left[\sqrt{2E_i} - \sqrt{2(E_i - \Delta E)} \right] / 1.26. \quad (11)$$

For example, $\Delta A_r = 0.15$ for $E_i = 75$ eV and $I = 3 \times 10^{14}$ W/cm^2.

The parallel momentum distributions for single ionization of He$^+$ from all excited states of $n=2$ and 3 are calculated by solving the TDSE. Calculations were performed for a wide intensity range from 1.8 to 4.5×10^{14} W/cm^2 with a step of 0.1×10^{14} W/cm^2. To get the parallel momentum distributions along the polarization direction of the laser field, we first evaluate the two-dimensional (2D) momentum distributions for the ionized electrons. The 2D photoelectron momentum distributions parallel and perpendicular to the laser polarization direction for single ionization of He$^+$ from excited states of $2p_0$ and $3p_0$ in an 800 nm laser field at the intensity of 2.5×10^{14} W/cm^2 are displayed in Figs. 3(a) and 3(b), respectively. In Fig. 3(c) we show the electric field used in TDSE calculations, which is expressed by

$$\boldsymbol{F}(t) = a(t)F_0 \cos(\omega t + \phi)\hat{z}, \quad (12)$$

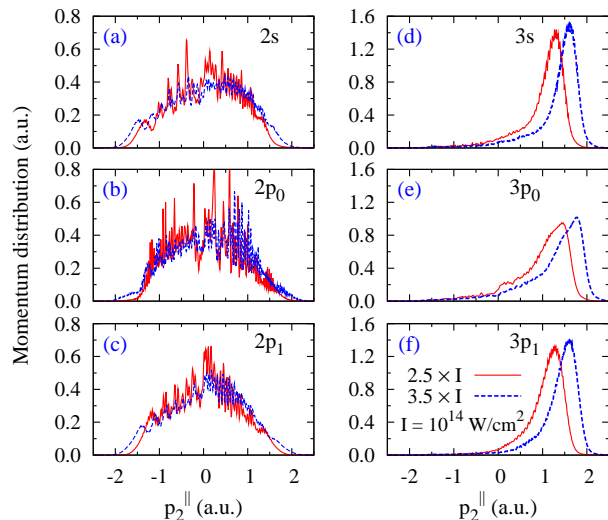where the envelope $a(t)$ is chosen to be one for the first five cycles and ramped off over three cycles. Here, to

FIG. 4: Parallel momentum distributions for the electron ionized from He$^+$ in the excited states of (a) $2s$, (b) $2p_0$, (c) $2p_1$, (d) $3s$, (e) $3p_0$, and (f) $3p_1$ by an 800 nm laser field at peak intensities of 2.5 and 3.5×10^{14} W/cm^2, respectively.

save computing time, we chose a shorter pulse than that used in the experiment due to the fact that electrons in the excited states are quickly ionized in the electric field. In addition, the carrier envelope phase ϕ is set to $\pi/2$ to account for the recollision process in which the laser-induced recolliding electron returns to the origin along the $-\hat{z}$ direction.

By integrating the 2D momentum distributions over the momentum component perpendicular to the direction of laser polarization, one obtains the parallel momentum distributions for electrons subsequently ionized in the laser field from the excited states due to laser-induced recollision. Figure 4 shows selected TDSE results for single ionization of He$^+$ from the $2s$, $2p_0$, $2p_1$, $3s$, $3p_0$, and $3p_1$ excited states in a laser field with peak intensities of 2.5 and 3.5×10^{14} W/cm^2, respectively. First of all, by integrating the distributions over the parallel momentum, we found that the total single ionization yields for all cases considered here are close to unity, indicating that essentially all excited atomic ions are further ionized. Secondly, the momentum distributions are not symmetric with respect to $p_2^{||} = 0$, especially for higher excited states. This is not surprising, since the 2D momentum distributions produced by the TDSE are asymmetric with respect to $p_{||} = 0$, as shown in Figs. 3(a) and 3(b). Thirdly, the parallel momentum distributions spread outside of A_0, where A_0 is the maximum value of vector potential. For the intensities of 2.5 and 3.5×10^{14} W/cm^2, A_0=1.48 and 1.76, respectively. This is also owing to the 2D momentum distributions beyond the range of $2U_p$, as indicated by the half circle in Figs. 3(a) and 3(b). As demonstrated in Figs. 3(a) and 3(b), several backscattering rings, due to elastic collisions of the

returning electron with the parent ion, appear around $2U_p$ in the 2D photoelectron momentum distributions, indicating a clear transition from direct to recollision. However, the enhancement occurring around $2U_p$ in the photoelectron spectra obtained from *ab initio* solution of TDSE in Keil *et al.* [44] for some laser and target parameters does not occur in the present calculations. By introducing the scaling factor $\alpha_C = Z/\sqrt{\omega}$ for the Coulomb potential and the scaling factor $\alpha_L = F_0/\omega^{3/2}$ for the laser field in the TDSE, Keil *et al.* found that the enhancement around twice the ponderomotive energy in the photoelectron spectra due to soft recollision can occur only when $\alpha_C/\alpha_L > 1$. For the cases considered here, $\alpha_C/\alpha_L = 0.67$, the contributions from recollision are at least two orders smaller than the direct ionization, and hence can be safely ignored.

While the numerical solution of the TDSE provides accurate results, the intrinsic deficiency of the TDSE calculations is that insight into the underlying physics may be hidden. On the other hand, the principal physics of tunneling ionization can be directly unveiled by the ADK model, in which the ionization rate, with the depletion effect taken into account, can be expressed as

$$Y_I^{\text{ADK}}(t) = W\left[|F(t)|\right] e^{-\int_{t_0}^t W\left[|F(t')|\right]dt'}, \quad (13)$$

where $W\left[|F(t)|\right]$ is the modified ADK rate given by Eq. (2) in Ref. [23].

In Fig. 5(a), we show the ionization rate $Y_I^{\text{ADK}}(t)$ of He$^+$ from $2p_0$ in an 800 nm laser field at peak intensities of 2.0 and 3.0×10^{14} W/cm^2, respectively. Note that the integral of $Y_I^{\text{ADK}}(t)$ over time yields the total ionization probability, i.e.,

$$P = \int_{t_0}^t Y_I^{\text{ADK}}(t)dt = 1 - e^{-\int_{t_0}^t W\left[|F(t')|\right]dt'}. \quad (14)$$

According to the classical rescattering model, tunneling ionization starts as soon as the laser-induced recollision takes place by which the parent ion is promoted to an excited state. For simplicity, a monochromatic laser field was used to produce Fig. 5(a), and the tunneling ionization was set to start at the time t_r when the electric field $F_r = 0$ and $A_r = -A_0$, where A_0 is the maximum value of the vector potential. One can see that all the excited atomic ions are ionized within half an optical cycle in the subsequent strong laser field for a peak intensity of 3.0×10^{14} W/cm^2. For a laser field with the lower intensity of 2.0×10^{14} W/cm^2, ionization continues for a longer time, but still essentially ceases within one optical cycle.

Assuming that the initial velocity of the tunneling electron can be neglected, the momentum spectrum for single ionization of the parent ion is given by

$$D_I^{\text{ADK}}(p_2^{||}) = D_I^{\text{ADK}}[-A(t)] = \frac{1}{|E(t)|}Y_I^{\text{ADK}}(t). \quad (15)$$

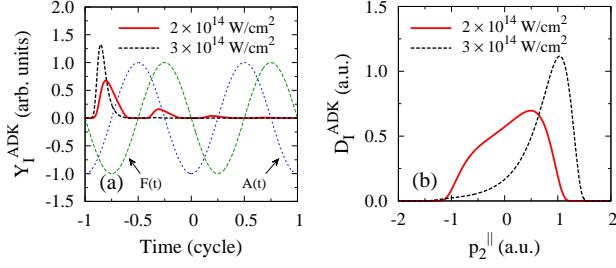Using Eq. (15), we calculated the parallel momentum distributions corresponding to the ADK rates shown in

FIG. 5: (a) ADK rate for ionization of He$^+$ from $2p_0$ vs. time in 800 nm laser fields with peak intensities of 2.0 and 3.0×10^{14} W/cm^2, respectively. The electric field and vector potential of the laser field, both normalized to unity, are also indicated. (b) Parallel momentum distributions corresponding to the ADK rates shown in (a).

Fig. 5(a). The results are displayed in Fig. 5(b). The parallel momentum distributions from the ADK model for ionization of He$^+$ from $2p_0$ are very different from those obtained with the TDSE shown in Fig. 4(b). However, they are similar to the TDSE results for ionization of He$^+$ from $n = 3$, which are highly asymmetric (c.f. Figs. 4(d-f)). From Fig. 5(a), we see that the high asymmetry of the parallel momentum distributions is due to the fast tunneling ionization lasting for less than half an optical cycle, while the asymmetry is reduced when tunneling ionization occurs for a longer time. The substantial discrepancies between TDSE and ADK in the parallel momentum distributions, as displayed in Figs. 4 and 5, suggest that the ADK tunneling model might not apply for electron ionization from excited states of atomic ions due to the low ionization potentials.

We emphasize that the modified ADK model was only employed here to provide some insight into the asymmetric parallel momentum distributions generated by solving the TDSE shown in Fig. 4. It was not adopted in the numerical simulations for the CMD in the present paper, since for tunneling ionization considered here, the excited states of He$^+$ require special treatment due to the Coulomb degeneracy [45, 46].

With the well-prepared parallel momentum distributions from the R-matrix and TDSE calculations for the two outgoing electrons, respectively, we are ready to calculate the CMD using Eq. (8). Figure 6 displays the correlated parallel momentum spectra for tunneling from the excited $2s$, $2p_0$, $2p_1$, $3s$, $3p_0$, and $3p_1$ states in a laser field with a peak intensity of 3.5×10^{14} W/cm^2. It should be noted that the CMDs plotted in Fig. 6 are for the situation in which the laser-induced electron returns to the parent ion along the direction of $-\hat{z}$. The pattern of the CMD directly reflects the momentum distributions of the returning electron after recollision and of the tunneling-ionized electron from excited states of the parent ion. For instance, in Fig. 6(e), the dense population in the region of small $p_1^{\parallel}$ and large $p_2^{\parallel}$ results from strong forward scattering of the returning electron from the parent ion and
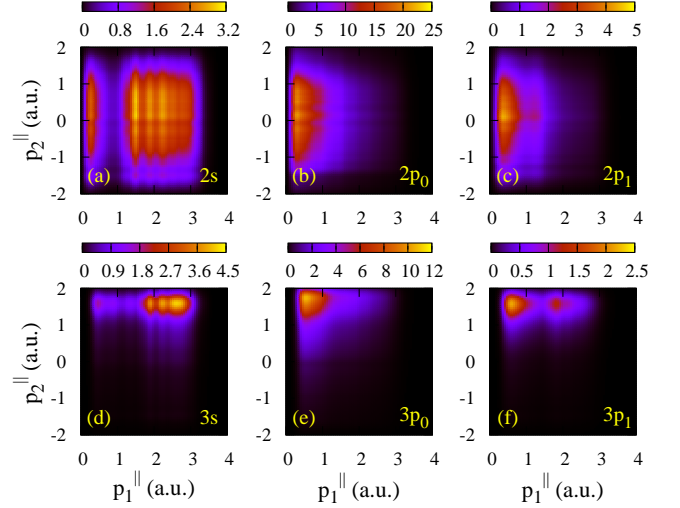

FIG. 6: Right-side ($p_1^{\parallel} > 0$) correlated parallel momentum spectra for excitation tunneling from (a) $2s$, (b) $2p_0$, (c) $2p_1$, (d) $3s$, (e) $3p_0$, and (f) $3p_1$ in an 800 nm laser field at a peak intensity of 3.5×10^{14} W/cm^2.
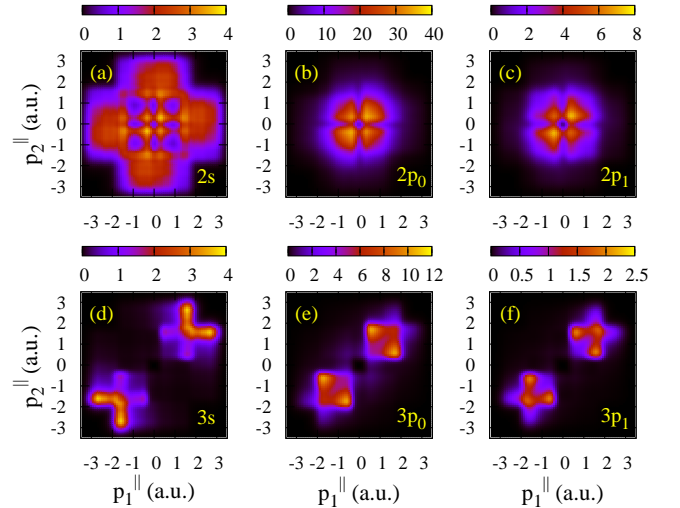

FIG. 7: Symmetrized full-space correlated parallel momentum spectra for excitation-tunneling from the excited states of (a) $2s$, (b) $2p_0$, (c) $2p_1$, (d) $3s$, (e) $3p_0$, and (f) $3p_1$ in an 800 nm laser field at a peak intensity of 3.5×10^{14} W/cm^2.

the fast tunneling ionization of the electron from the excited state. Note that in the CMD presented in Fig. 6, the contributions from collisions at all possible incident energies were accounted for.

So far, we have only considered the situation in which the laser-induced electron returns to the parent ion along the $-\hat{z}$ direction. In this case the returning electron is tunnel-ionized in the half cycle when the electric field is negative [47]. Since the laser field only defines an alignment but not an orientation for long pulses, as those considered here, the laser-induced electron born in the
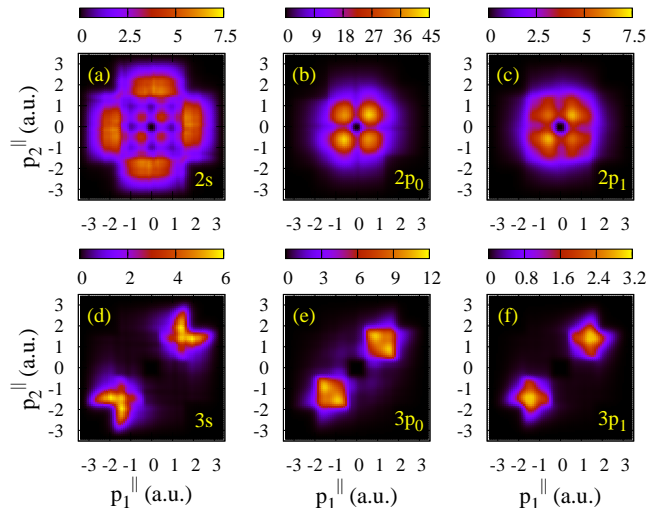
FIG. 8: Focal-volume-averaged correlated parallel momentum spectra for excitation-tunneling from the excited states of (a) $2s$, (b) $2p_0$, (c) $2p_1$, (d) $3s$, (e) $3p_0$, and (f) $3p_1$ in an 800 nm laser field at the peak intensity of 3.5×10^{14} W/cm^2.
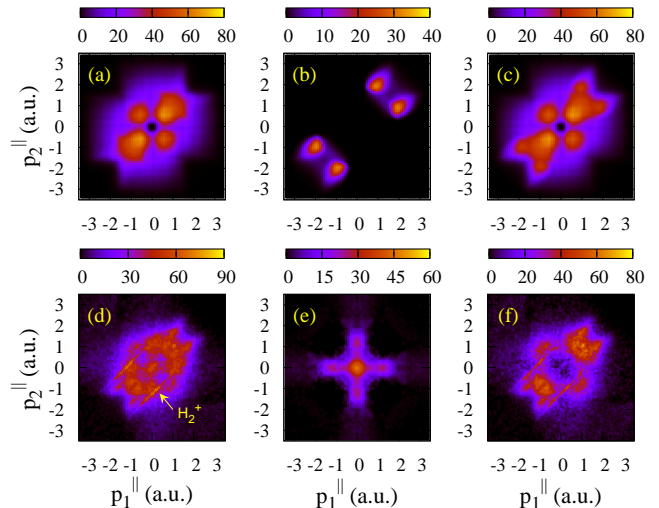

FIG. 9: Comparison of the simulated correlated parallel momentum spectra with the experimental measurements. The first row shows the simulated results for NSDI of He in the laser field at the peak intensity of 3.5×10^{14} W/cm^2: (a) Excitation-tunneling from all excited states of $n = 2$ and 3, (b) $(e, 2e)$, (c) sum of excitation-tunneling and $(e, 2e)$. The second row displays the experimental data: (d) Full experimental measurements, (e) spectra excluding $(e, 2e)$ and excitation-tunneling, (f) spectra deduced from (d) with (e) deducted. The calculations include the integration over the focal volume of the laser.

other half cycle, when the electric field is positive, possesses the same probability for returning to the parent ion along the $+\hat{z}$ direction. The two half cycles of the laser field yield opposite drift momenta. Furthermore, due to the indistinguishability of the two outgoing electrons, the CMD for excitation-tunneling should be symmetric with respect to both diagonals $p_1^{||} = \pm p_2^{||}$. For the excitation-tunneling mechanism, however, the additional symmetry with respect to the coordinate axes, suggested by Feuerstein *et al.* [5], is not guaranteed. Figure 7 depicts the full-space CMD for excitation-tunneling upon symmetrization of the CMD displayed in Fig. 6. One clearly sees that the distributions are not symmetric with respect to the coordinate axes, especially for tunneling ionization of the second electron from highly-excited states, as shown in Figs. 7(d-f). This is, again, due to the fast tunneling ionization discussed above.

In order to compare our predictions with experiment, an integration over the focal volume has to be performed. In Fig. 8 we present the focal-volume-averaged CMD for excitation-tunneling from the excited $2s$, $2p_0$, $2p_1$, $3s$, $3p_0$, and $3p_1$ states in an 800 nm laser field at a peak intensity of 3.5×10^{14} W/cm^2. While the principal patterns remain almost the same, focal-volume averaging yields observable differences from the patterns displayed in Fig. 7.

Finally, in Fig. 9 we present a direct comparison between the simulated results and the experimental data. Figure 9(a) depicts the CMD for excitation-tunneling in NSDI of helium. These results were obtained by summing over all distributions corresponding to the situation in which the initially released electron promotes the second electron in the ground state of He$^+$ to all possible excited states of $n = 2$ and $n = 3$, each of which

is specified with angular momentum and magnetic quantum number. Nevertheless, with the calculated CMD for excitation-tunneling only, one is not ready to compare with the entire correlated electron spectra measured in the experiment, unless the momentum distribution for the recollisional $(e, 2e)$ process is also considered.

Very recently, we revisited the NSDI of helium [41] focusing on the fingerlike structure observed in the experiment of Staudte *et al.* [7]. That structure is attributed to the recollisional $(e, 2e)$ process. In Ref. [41], several theoretical models were employed to calculate the triple-differential cross sections for electron impact ionization of He$^+$. It was found that, among those models, the so-called DS4C model achieves the best agreement with the experimental data. In the DS4C model, both the pre-collision Coulomb interaction between the incident electron and the parent ion and the postcollision Coulomb interaction between the two outgoing electrons are taken into account. Furthermore, the dynamic screening (DS) of the three-body Coulomb interactions in the final state, due to the fact that the strength of the interaction of any two particles is affected by the presence of the third one, is considered. Figure 9(b) displays the CMD for the contributions from $(e, 2e)$ simulated by Chen *et al.* using the DS4C model [41]. Focal-volume-averaging was performed and the lowering of the threshold due to the presence of the electric field at the moment of recollision was taken into account.

The calculated CMD for NSDI of He including both recollisional ionization and excitation-tunneling are displayed in Fig. 9(c), and the entire correlated electron spectra obtained experimentally are plotted in Fig. 9(d). The absence of populations along the axes in the experimental CMD in Fig. 9(d) in the simulated distributions in Fig. 9(c) is not surprising, since an analysis based on the rescattering model shows that the kinematically allowed regime for the correlated electron momentum components parallel to the laser polarization axis in excitation-tunneling does not reach this region for the case considered here, even with the potential change taken into account (see Fig. 3 in Ref. [19]). This implies that, apart from the laser-induced recollisional ionization and excitation-tunneling, other mechanisms might be involved in the NSDI process. In Ref. [19], an additional mechanism was suggested to account for the distribution along the axes in the CMD. This mechanism is referred to as capture-tunneling, in which the returning electron is captured by dielectronic recombination with the He$^+$(1s) ion to form a doubly-excited state. Then the two electrons in such doubly-excited states are easily tunnel-ionized in the laser field, thereby contributing to NSDI. Based on this scenario, the distribution due to capture-tunneling can be separated from the entire correlated electron spectra measured in the experiment. This is displayed in Fig. 9(e) (see also Fig. 11(c) in Ref. [19]). Deducting the distribution due to capture-tunneling from the entire measured correlated electron spectra, one obtains the "refined" experimental CMD owing to the mechanisms of recollisional ionization and excitation-tunneling only, as shown in Fig. 9(f).

Based on the above discussions, the calculated CMD for NSDI of helium including both recollisional $(e, 2e)$ and excitation-tunneling displayed in Fig. 9(c) should be compared with the corresponding experimental data shown in Fig. 9(f). The theoretical predictions are in fairly good agreement with experiment. Nevertheless, to achieve the best overall agreement, the peak intensity chosen in the present calculation was 3.5×10^{14} W/cm^2, while it was estimated as 4.5×10^{14} W/cm^2 in the experiment. In spite of the overall good qualitative agreement, discrepancies between the simulated results and the experimental data still exist. For example, the distributions predicted by the present model spread to larger momenta along the main diagonal than those seen in the experiment. However, while the experimental data were symmetrized by exchanging the two electron indices due to the indistinguishability of the electrons [7], one can observe a clear asymmetry with respect to the antidiagonal $p_1^\| = -p_2^\|$. This asymmetry suggests potential experimental artifacts. In light of these issues, we regard the overall agreement between theory and experiment as satisfactory.

The fairly good agreement achieved between the simulated results and experiment, as shown in Figs. 9(c) and 9(d), is partially due to the asymmetric distribution of excitation-tunneling in Fig. 9(c). This asymme-
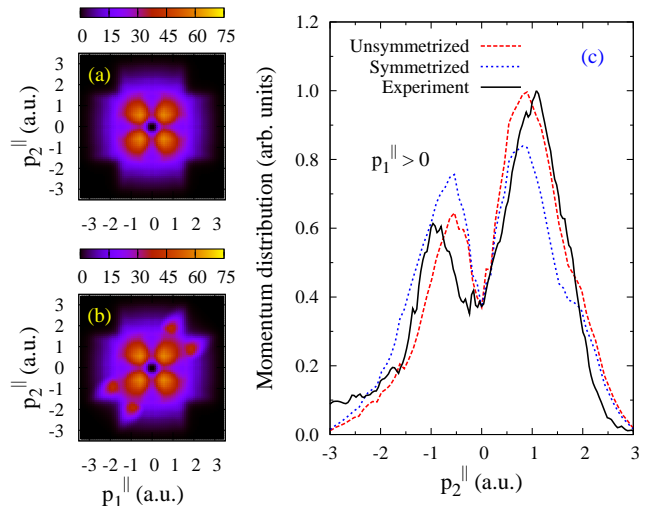

FIG. 10: (a) Artificially symmetrized correlated parallel momentum spectra of Fig. 9(a) for excitation-tunneling; (b) Sum of excitation-tunneling in (a) and $(e, 2e)$ in Fig. 9(b); (c) Momentum distributions obtained by projecting the correlated momentum distributions onto $p_2^\|$ for $p_1^\| > 0$. The (black) solid and (red) broken curves represent the results obtained from Fig. 9(f) for the experiment and Fig. 9(c) for the simulations, respectively, and the (blue) dotted line is obtained from the data in (b). The theoretical results are normalized to the dip of the experimental data for comparison.

try originates from the asymmetric parallel momentum distributions calculated by solving the TDSE for the electron ionized from the excited states, as shown in Fig. 4. It should be mentioned that, in a previous paper [19], the parallel momentum distributions for electrons ionized from the excited states evaluated by using the ADK model were artificially symmetrized according to the scenario that the CMD for excitation-tunneling in NSDI should be symmetric with respect to the coordinate axes. This scenario, however, is believed to be not always true; see Ref. [48] for example. This implies that forced symmetrization of the CMD for excitation-tunneling is not appropriate. However, in order to see how much difference it would make to the comparison displayed in Fig. 9 if the excitation-tunneling turned out to be symmetric with respect to the coordinate axes, we artificially symmetrized the CMD in Fig. 9(a) for excitation-tunneling, and the results are shown in Fig. 10(a). Consequently, as displayed in Fig. 10(b), the CMD for NSDI of He including both recollisional ionization and excitation-tunneling can then be obtained by adding the contributions from $(e, 2e)$ in Fig. 9(b) to those for excitation-tunneling in Fig. 9(a). One can see that obvious discrepancies exist between the CMDs in Figs. 9(c) and 10(b). As a result, the agreement between the experimental data in Fig. 9(f) and the artificially symmetrized simulated spectra in Fig. 10(b) becomes worse. Furthermore, to present a direct quantitative comparison of our model simulations with experiment, we performed the integral of the

CMDs in Figs. 9(c), 9(e) and 10(b) over the parallel momentum $p_1^{||}$ for $p_1^{||} > 0$, and the obtained results are compared in Fig. 10(c). It is clearly seen that the heights of the two peaks in the experimental momentum distributions are well predicted by the QRS model without symmetrizing the CMD for excitation-tunneling with respect to the coordinate axes, while symmetrization leads to higher peak for $p_2^{||} < 0$ and a lower peak for $p_2^{||} > 0$ compared with experiment.

IV. SUMMARY AND OUTLOOK

We revisited the NSDI experiment on helium performed by Staudte *et al.* [7], focusing on the process of recollisional excitation-tunneling. By including the predicted results for the recollisional $(e, 2e)$ process [41], we presented a direct comparison of our model calculations with the experimental data and find that our model reproduces the experimental findings to a very satisfactory degree. The theoretical methods used in the present paper are based on the improved QRS model, in which the potential change due to the presence of an electric field at the instant of recollision has been taken into account. In the numerical simulations of the correlated two-electron momentum distributions for excitation-tunneling, the parallel momentum distributions for the returning electron after recollision were obtained from the differential cross sections for electron impact excitation of He$^+$ evaluated using the nonperturbative R-matrix (close-coupling) method, while the parallel momentum distributions for the tunneling electron were calculated by solving the TDSE. The correlated two-electron momentum distributions for excitation-tunneling were found to be not symmetric with respect to the coordinate axes, in contrast

to the scenario suggested in Ref. [5]. This asymmetry is attributed to the fast tunneling ionization of electrons in the excited states.

All our theoretical treatments are based on accurate, fully quantum mechanical calculations. The deficiency of the present model remains that it is still hard to predict the momentum distributions for capture-tunneling, although the mechanism can be interpreted qualitatively. Even though it was not done in the present paper, we emphasize that our work opens a way to study the interference effect in NSDI within the framework of the QRS model, since both the R-matrix and TDSE solutions not only provide the probabilities but also the necessary amplitudes.

[1] B. Walker, B. Sheehy, L. F. DiMauro, P. Agostini, K. J. Schafer, and K. C. Kulander, Phys. Rev. Lett. **73**, 1227 (1994).

[2] Th. Weber, M. Weckenbrock, A. Staudte, L. Spielberger, O. Jagutzki, V. Mergel, F. Afaneh, G. Urbasch, M. Vollmer, H. Giessen, and R. Dörner, Phys. Rev. Lett. **84**, 443 (2000).

[3] R. Moshammer, B. Feuerstein, W. Schmitt, A. Dorn, C. D. Schröter, J. Ullrich, H. Rottke, C. Trump, M. Wittmann, G. Korn, K. Hoffmann, and W. Sandner, Phys. Rev. Lett. **84**, 447 (2000).

[4] P. B. Corkum, Phys. Rev. Lett. **71**, 1994 (1993).

[5] B. Feuerstein, R. Moshammer, D. Fischer, A. Dorn, C. D. Schröter, J. Deipenwisch, J. R. Crespo Lopez-Urrutia, C. Höhr, P. Neumayer, J. Ullrich, H. Rottke, C. Trump, M. Wittmann, G. Korn, and W. Sandner, Phys. Rev. Lett. **87**, 043003 (2001).

[6] T. Weber, H. Giessen, M. Weckenbrock, G. Urbasch, A. Staudte, L. Spielberger, O. Jagutzki, V. Mergel, M. Vollmer, and R. Dörner, Nature **405** 658 (2000).

[7] A. Staudte, C. Ruiz, M. Schöffler, S. Schössler, D. Zeidler, Th. Weber, M. Meckel, D. M. Villeneuve, P. B. Corkum, A. Becker, and R. Dörner, Phys. Rev. Lett. **99**, 263002 (2007).

[8] A. Rudenko, V.L.B. de Jesus, Th. Ergler, K. Zrost, B. Feuerstein, C. D. Schröter, R. Moshammer, and J. Ullrich, Phys. Rev. Lett. **99**, 263003 (2007).

[9] Y. Liu, S. Tschuch, A. Rudenko, M. Dürr, M. Siegel, U. Morgner, R. Moshammer, and J. Ullrich, Phys. Rev. Lett. **101**, 053001 (2008).

[10] Y. Liu, D. Ye, J. Liu, A. Rudenko, S. Tschuch, M. Dürr, M. Siegel, U. Morgner, Q. Gong, R. Moshammer, and J. Ullrich, Phys. Rev. Lett. **104**, 173002 (2010).

[11] B. Bergues, M. Kübel, N. G. Johnson, B. Fischer, N. Camus, K. J. Betsch, O. Herrwerth, A. Senftleben, A. M. Sayler, T. Rathje, T. Pfeifer, I. Ben-Itzhak, R. R. Jones, G. G. Paulus, F. Krausz, R. Moshammer, J. Ullrich, and M. F. Kling, Nat. Commun. **3**, 813 (2012)

[12] M. Kübel, K. J. Betsch, N. G. Kling, A. S. Alnaser, J. Schmidt, U. Kleineberg, Y. Deng, I. Ben-Itzhak, G.

G. Paulus, T. Pfeifer, J. Ullrich, R. Moshammer, M. F. Kling, and B. Bergues, New J. Phys. **16**, 033008 (2014).

[13] D. F. Ye, X. Liu, and J. Liu, Phys. Rev. Lett. **101**, 233003 (2008).

[14] Y. Zhou, Q. Liao, and P. Lu, Phys. Rev. A **82**, 053402 (2010).

[15] Z. Chen, Y. Liang, and C. D. Lin, Phys. Rev. Lett. **104**, 253201 (2010).

[16] Z. Chen, A.-T. Le, T. Morishita, and C. D. Lin, Phys. Rev. A **79**, 033409 (2009).

[17] Z. Chen, A.-T. Le, T. Morishita, and C. D. Lin, J. Phys. B **42**, 061001 (2009).

[18] A.-T. Le, R. R. Lucchese, S. Tonzani, T. Morishita, and C. D. Lin, Phys. Rev. A **80**, 013401 (2009).

[19] Z. Chen, Y. Liang, and C. D. Lin, Phys. Rev. A **82**, 063417 (2010).

[20] T. Morishita, A.-T. Le, Z. Chen, and C.D. Lin, Phys. Rev. Lett. **100**, 013903 (2008).

[21] Z. Chen, Y. Liang, D. H. Madison, and C. D. Lin, Phys. Rev. A **84**, 023414 (2011).

[22] M. V. Ammosov, N. B. Delone, and V. P. Krainov, Zh. Eksp. Teor. Fiz. **91**, 2008 (1986).

[23] X. M. Tong and C. D. Lin, J. Phys. B **38**, 2593 (2005).

[24] Y. Liang, Z. Chen, D. H. Madison, and C. D. Lin, J. Phys. B **44**, 085201 (2011).

[25] A. Scrinzi, M. Geissler, and T. Brabec, Phys. Rev. Lett. **83**, 706 (1999).

[26] X. Chu and S. I. Chu, Phys. Rev. A **63**, 013414 (2000).

[27] X. L. Hao, J. Chen, W. D. Li, B. Wang, X. Wang, and W. Becker, Phys. Rev. Lett. **112**, 073002 (2014).

[28] A. S. Maxwell and C. Figueira de Morisson Faria, Phys. Rev. A **92**, 023421 (2015); Phys. Rev. Lett. **116**, 143001 (2016).

[29] W. Quan, X. L. Hao, Y. L. Wang, Y. J. Chen, S. G. Yu, S. P. Xu, Z. L. Xiao, R. P. Sun, X. Y. Lai, S. L. Hu, M. Q. Liu, Z. Shu, X. D. Wang, W. D. Li, W. Becker, X. J. Liu, and J. Chen, Phys. Rev. A **96**, 032511 (2017).

[30] Z. Chen, Y. Zheng, W. Yang, X. Song, J. Xu, L. F. Di-

Mauro, O. Zatsarinny, K. Bartschat, T. Morishita, S. F. Zhao, and C. D. Lin, Phys. Rev. A **92**, 063427 (2015).

[31] Z. Chen, X. Li, O. Zatsarinny, K. Bartschat, and C. D. Lin, Phys. Rev. A **97**, 013425 (2018).

[32] H. W. van der Hart and K. Burnett, Phys. Rev. A **62**, 013407 (2000).

[33] T. Morishita, Z. Chen, S. Watanabe, and C. D. Lin, Phys. Rev. A **75**, 023407 (2007).

[34] G. L. Yudin and M. Y. Ivanov, Phys. Rev. A **64**, 035401 (2001).

[35] O. Zatsarinny and K. Bartschat, J. Phys. B 46, 112001 (2013).

[36] Y. Liang, Phys. Rev. A **82**, 055403 (2010).

[37] C. I. Blaga, J. Xu, A. D. DiChiara, E. Sistrunk, K. Zhang, P. Agostini, T. A. Miller, L. F. DiMauro, and C. D. Lin, Nature (London) **483**, 194 (2012).

[38] Z. Chen, J. Xu, W. Yang, and X. Song, Phys. Rev. A **88**, 065402 (2013).

[39] Z.-J. Chen, J.-M. Ye, and Y.-B. Yang, Chin. Phys. B **24**, 103203 (2015).

[40] T. Morishita and O. I. Tolstikhin, Phys. Rev. A **96**, 053416 (2017).

[41] Z. Chen, Y. Wang, L. Zhang, and X. Jia, Phys. Rev. A **99**, 033401 (2019).

[42] X. M. Tong and S. I. Chu, Chem. Phys. **217**, 119 (1997).

[43] S. Augst, D. D. Meyerhofer, D. Strickland, and S. L. Chin, J. Opt. Soc. Am. B **8**, 858 (1991).

[44] Th. Keil, S. V. Popruzhenko, and D. Bauer, Phys. Rev. Lett. **117**, 243003 (2016).

[45] T. Yamabe, A. Tachibana, and H. J. Silverstone, Phys. Rev. A **16**, 877 (1977).

[46] P. K. Samygin, T. Morishita, and O. I. Tolstikhin, Phys. Rev. A **98**, 033401 (2018).

[47] Z. Chen, T. Morishita, A.-T. Le, and C. D. Lin, Phys. Rev. A **76**, 043402 (2007).

[48] A. S. Maxwell and C. Figueira de Morisson Faria, Phys. Rev. A **92**, 023421 (2015).